Biofabrication

PAPER

Stratified tissue biofabrication by rotational internal flow layer engineering

Ian Holland[1,*], Wenmiao Shu[2,*] and Jamie A Davies[1]

[1] Deanery of Biomedical Science and the Centre for Engineering Biology, University of Edinburgh, Edinburgh, United Kingdom
[2] Department of Biomedical Engineering, University of Strathclyde, Glasgow, United Kingdom
* Authors to whom any correspondence should be addressed.

E-mail: iholland@exseed.ed.ac.uk and will.shu@strath.ac.uk

Keywords: microtissue biofabrication, rimming flow, tubular tissue, collagen, vascular tissue

Supplementary material for this article is available online

OPEN ACCESS

RECEIVED
15 December 2022

REVISED
21 June 2023

ACCEPTED FOR PUBLICATION
29 June 2023

PUBLISHED
19 July 2023

Abstract

The bioassembly of layered tissue that closely mimics human histology presents challenges for tissue engineering. Existing bioprinting technologies lack the resolution and cell densities necessary to form the microscale cell-width layers commonly observed in stratified tissue, particularly when using low-viscosity hydrogels, such as collagen. Here we present rotational internal flow layer engineering (RIFLE), a novel, low-cost biofabrication technology for assembling tuneable, multi-layered tissue-like structures. Using high-speed rotating tubular moulds, small volumes of cell-laden liquids added to the inner surface were transitioned into thin layers and gelled, progressively building macroscale tubes composed of discrete microscale strata with thicknesses a function of rotational speed. Cell encapsulation enabled the patterning of high-density layers (10^8 cells ml^{-1}) into heterogenous constructs. RIFLE versatility was demonstrated through tunica media assembly, encapsulating human smooth muscle cells in cell-width (12.5 μm) collagen layers. Such deposition of discrete microscale layers, facilitates the biofabrication of composite structures mimicking the nature of native stratified tissue. This enabling technology has the potential to allow researchers to economically create a range of representative layered tissue.

1. Introduction

Layered tissue is common throughout human anatomy, with notable examples found in cardiac [1], dermal [2], intestinal [3], retinal [4], alveolar [5] and vascular tissue [6]. Such stratification features a range of different cell types and extracellular matrices to create highly specialised, heterogeneous structures that imbue tissues with multiple properties and functions. Layered tissue follows the hierarchical structure of many other tissue types where microtissue units combine to form larger macrotissue structures [7]. Tissue engineering technologies, including biofabrication [8, 9], that intend to anatomically and functionally mimic native tissue often make extensive use of cells suspended in liquid-phase hydrogels that can be positioned and subsequently gelled [10]. Existing biofabrication technologies present advantages and disadvantages for researchers attempting to assemble stratified tissue. Inkjet bioprinting technologies typically have a low-cost and high resolutions [11] but are limited in the cell densities attainable [12] and unable to reach those observed in stratified tissue. Light based vat polymerisation methods, whilst also having excellent resolutions [13] currently require complicated material exchange procedures to create heterogeneous constructs [14], an important feature in many layered tissues. Extrusion bioprinting, the mainstay of research and industry [15], is able to deposit cell-laden hydrogels in a layer-by-layer fashion. However the technology suffers from low resolutions [16, 17], meaning it is unable to match those observed in stratified tissues, which can be often be the width or a cell or smaller [18]. The technology is further limited by the biofabrication printability window [19, 20] where hydrogels need to be extrudable through the nozzle, exhibit low filament spreading prior to

gelation and also maintain low shear stresses for cell survival. Consequently, a large amount of research effort is devoted to developing printable bioinks [15, 21], the properties of which are frequently aligned to the limitations of the printing technology rather than replicating the form of the target tissue. There remains a need for new biofabrication technologies that are able to form the complex microarchitecture of native tissue [22].

Recognising the challenges of using existing technologies to manipulate hydrogels into microscale layers, some researchers have attempted to develop improved biofabrication technologies. The sequential, dipping, spraying or direct extrusion of cell-laden hydrogels onto the external surface of cylinders to build up layers is one such strategy [23]. An advantage of this method resides in the formation of a tubular macroarchitecture, observed in many native layered tissues such as vascular, intestinal, tracheal, urethral and biliary tissue [24, 25]. Furthermore, cutting open tubular fabricated tissue allows simple conversion to planar structures [26], as would be needed to mimic dermal and retinal tissue. Rotation of the cylinder at high speeds under motor control [27, 28] enables a level of control over the layer thicknesses that is otherwise determined by the viscosity of the liquid hydrogel and the surface properties of the substrate layer [29]. A limitation of rod-based methods is the requirement to dip or spray cell solutions onto the external surface, necessitating large volumes of cell laden hydrogels that are ultimately wasted, inhibiting the cell densities attainable. Furthermore, in common with other bioprinting technologies, this approach has thus far been unable to assemble microscale layered tissue using collagen, the primary human extra cellular matrix (ECM) material. An innovative alternative method is centrifugal casting, where hydrogels are applied to the inside of a closed cylinder that is then rotated. Centrifugal forces push the hydrogel to coat the internal surface creating a tube, however layer thicknesses were limited to 1 mm as dictated by the volume added. The technology has received limited attention since the initial pioneering work by Mironov *et al* [26, 30, 31]. Centrifugation has also been more recently exploited as part of the sacrificial writing into functional tissue technology to create high-density macroscale constructs with microscale channels [32].

Building on these past examples, we present a novel biofabrication technology termed rotational internal flow layer engineering (RIFLE) that enables the rapid, high-resolution bioassembly of tuneable, microscale hydrogel and high-density cell layers into a macroscale tubular construct. By exploiting the fluid dynamic state of rimming flow, cell-laden hydrogels were suspended as microscale liquid layers on the internal surface of a rotating tube. The addition of a gelation process, such as an ionic crosslinking reagent or temperature change, gels the layer before the addition of further layers. Progressively, a multi-layered tubular structure is built up, mimicking the macro and microscale architectures of native tissues.

2. Materials and methods

2.1. RIFLE equipment and process

Multi-layered tubes were fabricated by using a 24 V DC motor (EC-i 30, Maxon Motor Ltd, UK) to rotate a clear acrylic tubular mould at high speeds. Motor speed was controlled using a DEC Module 24/2 (Maxon Motor), an Arduino microcontroller and a LabView (National Instruments, USA) program bespoke to the controller. Rotational speed in revolutions per minute (rpm) was determined through analysis of the digital outputs from the motor hall effect sensors using the same bespoke LabView program. With rotation set at the desired constant speed, liquid phase alginate (Protanal LF10/60FT, FMC Biopolymer, UK) was dropped onto the inner surface of the rotating mould using a 21 ga blunt-end needle (Fisnar, UK). The internal diameter of the rotating mould was 10 mm unless otherwise stated, with two 1 mm diameter drain holes located opposite one another. Rimming flow evenly distributed the fluid over the surface of the rotating mould, establishing a suspended thin layer of hydrogel, with excess fluid flowing out of the drain holes. The 100 mM $CaCl_2$ solution in H_2O (BDH chemicals, UK) was then added to the mould in a similar fashion, gelling the suspended alginate layer, with excess also flowing out of the drain holes. Repeated alginate and $CaCl_2$ addition sequentially built up a multi-layered tube. A smaller diameter stopper tube retained gelled layers within the mould. On completion the mould was removed from the motor and light tapping was sufficient to release tubes through the open end. Computer-aided design and animations were created using Autodesk Inventor Professional 2023 (Autodesk Inc. USA). Agarose multi-layered tubes were created in a similar fashion by dropping 40 °C liquid phase hydrogel onto the inner rotating surface. Rimming flow established a thin layer with excess fluid flowing out of the drain holes, as observed with alginate. Exposure to room temperature rapidly (<5 s) gelled the agarose layer before the addition of subsequent layers.

2.2. Rotational speed variation

Acellular tubes were fabricated using 1% (w/v) alginate or 1% (w/v) agarose, at rotational speeds of 4500, 6000, 7500 and 9000 rpm, with 3 independent replicates being made for each speed group. Images of each tube were captured with brightfield microscopy

with a ×4 objective using an Eclipse Ti2 microscope (Nikon Instruments Europe, Netherlands). Layer thicknesses were determined using ImageJ software by assigning a 100 μm wide selection box across the wall image and running the 'plot profile' function. Graphical visualisation of the profile enabled the relative positions of the layer boundaries to be discerned and individual layer thicknesses to be calculated and subsequently averaged.

2.3. Hydrogel concentration

Acellular tubes were fabricated at 9000 rpm using alginate concentrations of 0.5%, 1%, 2%, and 4% (w/v), or agarose at 1%, 2%, 4% and 8% (w/v), with 3 independent replicates being made for each concentration group. Images of each tube were captured using brightfield microscopy with a ×5 objective on a Zeiss Axiovert microscope (Zeiss, Germany). Layer thicknesses were determined as previously described.

2.4. Cell culture

Human embryonic kidney 293 T (HEK) cells were cultured in Dulbecco's Modified Eagle Medium (Gibco, 41966-029) supplemented with 10% foetal bovine serum (Gibco, 10270-106) and 1% Penicillin Streptomycin (Gibco, 15070-063). Human Aortic Smooth Muscle Cells (354-05A, Cell Applications, San Diego, USA) were cultured as a proliferative phenotype in Smooth Muscle Cell Growth Medium (311-500, Cell Applications) and used at passages below 5. All cells were cultured at 5% CO_2 and 37 °C.

2.5. Cell viability in alginate

Multi-layered tubes were formed with 1% alginate in PBS (Gibco 14190) at 9000 rpm. HEK cells were suspended in alginate at a density of 2.8×10^6 cells ml^{-1} and were included as a single central layer between acellular layers. Completed tubes were incubated in cell culture media at 5% CO_2 and 37 °C. Sections were removed from 3 separate tubes (n of 3) at 1, 4, 7 and 10 d after formation and a Live/Dead assay (Abcam, UK, ab115347) was performed according to manufacturer's instructions. Images were captured using an Eclipse Ti2 microscope (Nikon) with a ×20 objective. Viability was calculated as the ratio of the area of live and dead cells determined through the application of the ImageJ software 'make binary' and 'analyse particles' functions to the green (live) and red (dead) channel images [33]. The impact of centrifugation was assessed by rotating 3 populations of HEK cells, 300 μl, density 3.4×10^6 cells ml^{-1}, separately at 9000 rpm, suspended in media in a closed mould for 5 min. Cells were then immediately seeded for culture onto a 24 well plate. At 1, 4, 7 and 10 d after centrifugation a Live/Dead assay was performed and images taken as detailed previously.

2.6. Cell layer positioning

Flasks of HEK293 cells were pre-labelled red or green using cell tracker labels (C7025 and C34552, Thermofisher Scientific) or blue using Hoescht 33 342 (1:1000, H3570, Invitrogen, UK) according to manufacturer's instructions. Labelled cells were suspended in 1% (w/v) alginate in PBS and included in 9000 rpm bioassembled tubes. For adjacent patterned high-density cell layers HEK cell populations at a density of 1.0×10^8 cells ml^{-1} were included as a central band in varying patterns between acellular outer and inner layers. For rainbow patterns, red, green and blue labelled HEK293 cells in 1% (w/v) alginate were mixed in ratios matching the RGB values according to the ratios in table S2 creating 28 independent cell colour populations [34]. Tubes were sectioned and imaged in the sagittal plane using a Nikon A1R confocal inverted microscope in galvano scan mode with a ×4 or ×10 objectives and a ×4 tile scan mode for whole ring imaging. For spaced layer positioning HEK293 cells at a density of 2.7×10^6 cells ml^{-1} were layered between acellular layers with 10 or with 5 acellular layers between an outer green and an inner red population. Images were captured after 24 h of culture using an Eclipse Ti2 microscope (Nikon) using a ×4 or ×20 objective.

2.7. Mechanical testing

Plain, non-layered tubes were created by centrifugally casting 40 °C agarose 1% (w/v) in closed moulds at 7500 rpm and allowed to gel at room temperature. Layered tubes of the same total wall width were made using 1% (w/v) agarose, 7500 rpm, as previously detailed. Tube sections of 10 mm in length were mounted onto myograph wires (Livings Systems Instrumentation, USA) set 9 mm apart and allowed to equalise for 15 min. Sections, 3 from each group, were then stretched by 0.5 mm using the myograph micrometre (5.5% strain) and the resulting peak force and relaxation profile recorded for 10 min.

2.8. Collagen layer tube formation

The motor and rotational mould assembly were placed into a humidified chamber set at 37 °C. Collagen type I was prepared in small batches, transferred to a syringe on ice and used immediately to prevent premature gelation. The 445 μl Rat Tail collagen I at 3 mg ml^{-1} in 0.02 N acetic acid (Corning, USA) was neutralised with a 55 μl 2:1 ratio mixture of ×10 DMEM (Sigma D2429) and 0.4 M NaOH (Sigma S5881) and then 0.4 M NaOH dropwise until the phenol red in the DMEM indicated a neutral pH had been reached. Liquid phase collagen was dropped onto the inner rotating surface of the 4500 rpm rotating mould in the same fashion as alginate protocols and allowed to gel for 3 min before addition of the

next layer. Microscopy images were captured using an Eclipse Ti2 microscope (Nikon) using a ×4 objective.

2.9. Tunica media tissue assembly

For viability studies in collagen, human smooth muscle cells (hSMCs) were suspended in collagen at a density of 7.4 × 10^6 cells ml^{-1} and included as a single central layer between acellular layers. Completed tubes were incubated in cell culture media at 5% CO_2 and 37 °C. Sections were removed from 3 separate tubes (*n* of 3) at 1, 4, 7 and 10 d after formation and a Live/Dead assay (Abcam, UK, ab115347) was performed according to manufacturer's instructions. Images were captured using an Eclipse Ti2 microscope (Nikon) with a ×20 objective. The high difference in morphology and density between live, (spread, large and overlapping) and dead cells (rounded, small) prevented accurate quantification and viability was therefore only qualitatively analysed. For timelapse imaging hSMCs were included in a single layer at a density 1 × 10^6 cells ml^{-1} and brightfield images taken at 5 min intervals for 24 h immediately after bioassembly using a ×20 objective and an Eclipse Ti2 microscope (Nikon) with a stage top incubator. For cell orientation imaging hSMCs at a density of 0.6 × 10^6 were formed into 22 collagen layers and the tube placed over a rigid Ø8.5 mm mandrel to prevent over compaction. After 4 d the construct was removed from media, washed with PBS and fixed with 4% paraformaldehyde for 15 min at room temperature, before permeabilisation with 2% triton for 15 min at room temperature. Staining of actin filaments was achieved using Phalloidin-iFluor 594 (1:1000, ab176757, Abcam), nucelli were stained with Hoescht 33 342 (1:1000, H3570, Invitrogen, UK). Images were captured using a Nikon A1R confocal inverted microscope in galvano scan mode with a 10× objective and visualised using IMARIS software (Bitplane, Switzerland). For medial lamellar unit layer width determination, independent hSMC populations at a density of 1.5–2 × 10^6 cells ml^{-1} were included in collagen tubes with 10 or 20 layers spaced between them, 3 replicate tubes per spacing condition. After 24 h the constructs were fixed, stained with phalloidin and imaged as detailed previously. Confocal stacks were visualised and the distance between layers ascertained using the ImageJ 3D project function to rotate stacks through 90° to display the two layers in profile. The plot profile function was then applied to display the x positions of the peak fluorescent intensities from the two layers and the values subtracted from one another to calculate the total distance between layers.

2.10. Statistical analysis

All data are shown as the mean with ±standard deviation (SD). Statistical analysis was performed using a student's two tail *t* test.

3. Results and discussion

3.1. Development of the RIFLE process

The equipment and process are shown schematically in (figure 1(A)) and in the animation in supplementary movie 1. Initial process development was carried out using alginate hydrogel and calcium chloride crosslinker before moving onto agarose and then vascular tunica media tissue bioassembly with collagen. The addition of liquid phase alginate and calcium chloride into rotating closed cylinders failed to produce multiple layers due to variable hydrogel volume addition forming inconsistent thicknesses and because there was no route for the excess gelation agent to escape. The design of the mould was therefore modified to include drain holes to allow excess fluid to flow out of the cylinder. Liquid remaining within the cylinder was suspended as a thin, stable film on the rotating surface in a fluid dynamic process known as rimming flow [35]. A stopper tube fitted into the end of the tubular moulding ensured that outflow of excess fluid was possible only through the drain holes and also constrained the gelled layers within the tube. A component and reagent list can be found in supplementary information, table S1.

Alginate hydrogel drops were observed landing on and then spreading over the inner rotating mould surface before excess liquid exited through the drain holes. A similar process was then observed for crosslinker calcium chloride, which gelled the previously applied alginate layer. Repeated alternate applications of alginate and calcium chloride built up a layered tube. The use of a range of moulds of various inner diameters allowed the assembly of example tubes of different diameters (figure 1(B)). Brightfield microscopy of tube walls revealed stratified microscale layers (figure 1(C)). A layered tube took less than 20 min to produce and required a low volume of hydrogel: a Ø10 mm, 35-layer tube formed at 9000 rpm used 1.5 ml of 1% (w/v) alginate.

The observed rimming flow transition of the liquid from drops to thin layers on the internal rotating surface is most widely known in the industrial process of rotational moulding, where molten plastics are formed into large scale, single layer, hollow components [36]. Liquids rotated in a mould at high speeds will transition into rimming flow, suspending a uniform layer of liquid across the inner surface [37]. Here we have applied this principle to the formation of multi-layered hydrogel tubes, whilst allowing excess fluid a route to escape using drain holes. The fluid dynamics of rimming flow in closed cylinders has been studied extensively from a theoretical perspective [35, 38, 39] and experimentally [40, 41]. However, to our knowledge, no study has included the use of drain holes to allow the flow of excess liquid from the cylinder to establish thin

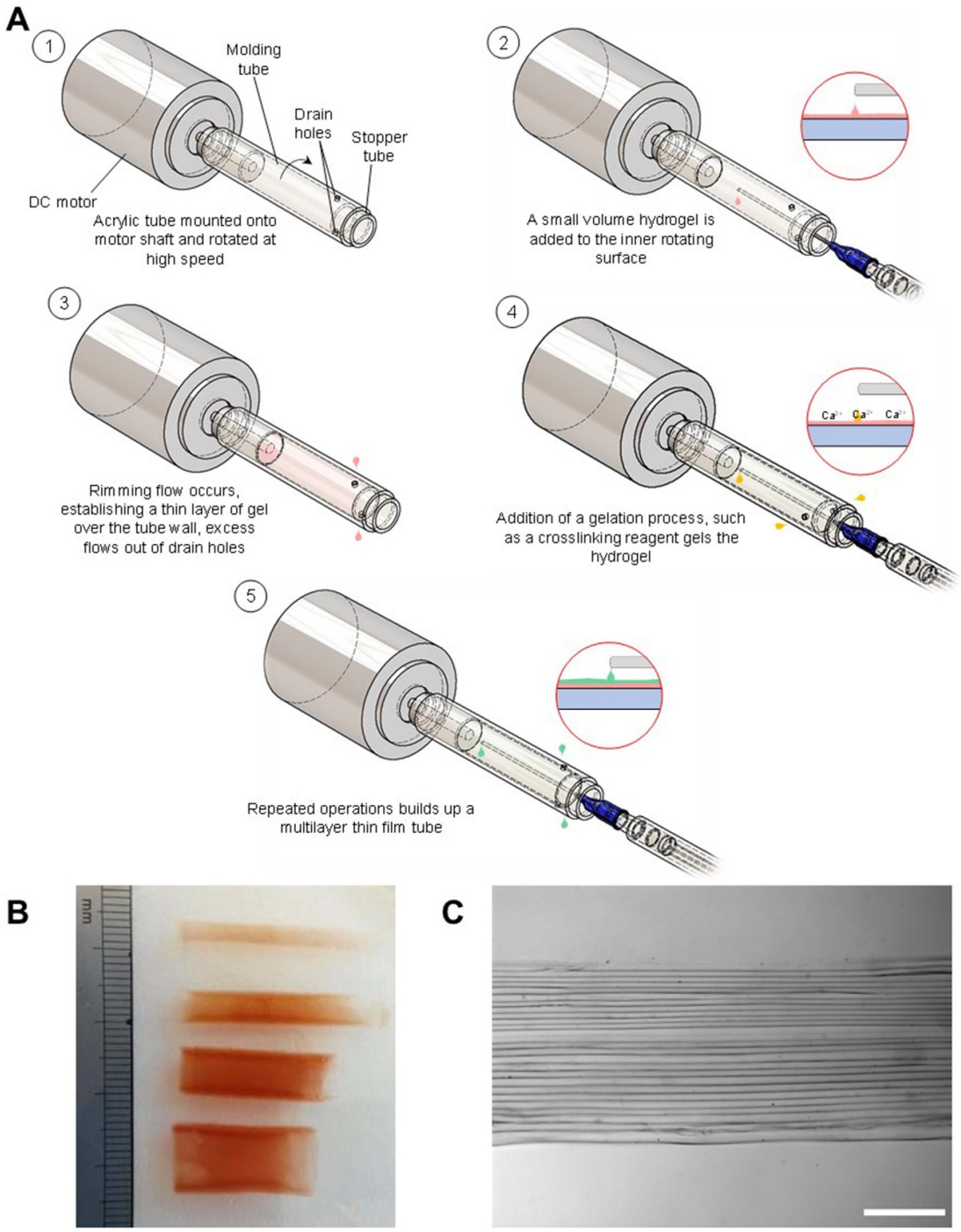

Figure 1. Illustration of RIFLE equipment and process. (A) Schematic representation of the RIFLE process. (B) Layered alginate tube size examples formed from moulds of different internal diameters, note: red food dye added to alginate to improve visualisation. (C) Brightfield microscopy image of a tube wall showing discrete alginate layers, white scale bar is 500 μm.

layers or to use it as a method for forming microscale multi-layered structures. The introduction of the drain holes changes the nature of the hydrogel flow inside the cylinder from a static centrifugal casting one, as previously published [26, 30, 31], into a dynamic one. The importance of this in a biofabrication context is that multiple microscale thin layers can be formed that mimic the anatomy of human stratified tissue, whereas centrifugal casting has only been shown to form single macroscale hydrogel layers.

3.2. Rotational speed and layer thicknesses

Rotational speed is a key parameter for the industrial process of rotational moulding [36] and in studies investigating the rimming flow behaviour of liquids in rotating closed cylinders [37, 42]. We aimed to determine whether the rotational speed of the moulding tube influenced the thickness of the layers formed. Layered alginate and agarose tubes were made at speeds of 4500, 6000, 7500 and 9000 rpm. Layer thicknesses were found to be a function of the speed of

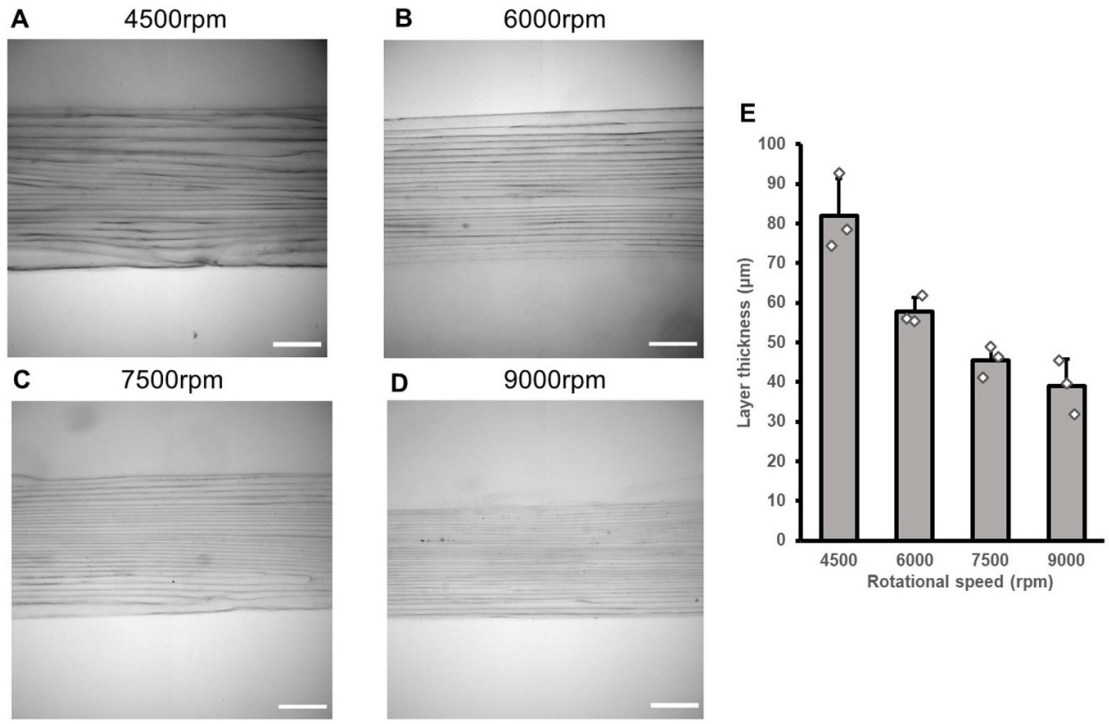

Figure 2. Layer thicknesses for RIFLE are determined by the speed of rotation. Brightfield microscopy images of tube walls formed using alginate 1% (W/V) at various rotational speeds. Scale bars are 500 μm. (A) 4500 rpm, (B) 6000 rpm, (C) 7500 rpm and (D) 9000 rpm. (E) Plot of layer thicknesses for rotational speed variation. Mean with error bars $\pm$SD $n = 3$.

rotation: microscopy images of alginate layers in tubes formed at different speeds are shown in (figure 2) and agarose in (figure S1). Analysis of the layer thicknesses revealed that increasing rotational speeds formed thinner layers (figures 2(E) and S1(E)).

As previously stated, no directly comparable theoretical or experimental fluid dynamic study is available. However, higher rotational speeds have been shown to reduce the thickness of layers for liquids adhered to the external surface of rods [27, 28, 37] and also to promote the even spreading of molten plastics in rotationally moulded parts [43]. It is reasonable to assume similar fluid dynamic effects influence the thickness of the layers formed in multilayer constructs made using RIFLE. Rotational speed variation therefore provided a method of controlling layer thickness and thus the microscale dimensions of bioassembled stratified tissue. Such dimensional tunability is an important feature when attempting to mimic native stratified tissue with a range of layer thicknesses found in different examples.

3.3. Hydrogel concentration and layer thicknesses

The concentration of liquid-phase hydrogels has been shown to influence multiple properties of biofabricated constructs, including elasticity, degradation and the behaviour of encapsulated cells [44]. Alginate concentrations of 4%, 2%, 1% and 0.5% (w/v) and agarose concentrations of 8%, 4%, 2% and 1% were used to form stratified tubular structures (figures 3 and S2). Analysis of the layer thicknesses revealed that the usage of higher percentage composition hydrogels resulted in tubes composed of thicker layers (figures 3(E) and S2(E)). Higher percentage concentration alginates and agaroses are more viscous [45, 46], establishing a positive correlation with between layer thickness and viscosity. Higher viscosity materials have previously been shown to require greater speeds to make the transition to rimming flow in both closed cylinder experiments [47] and theoretical models [37]. High viscosity alginates are likely to require greater centrifugal forces to form thinner layers.

Hydrogel concentration is a key factor when considering the degradation profile of the biofabricated tissue in a physiological environment, with desired faster or slower rates determined by the specific study or therapeutic objectives [48]. However, when seeking to use low viscosity hydrogels, such as low concentration alginate, collagen or decellularised extracellular matrix bio-inks [49, 50], researchers often find that they are unable to form microscale features using traditional bioprinting methods. A compromise between the desired hydrogel properties for tissue functionality and printability for the biofabrication technology is often needed [44, 45]. The presented system is able to form the microscale feature of layers using low viscosity alginate by suspending the liquid

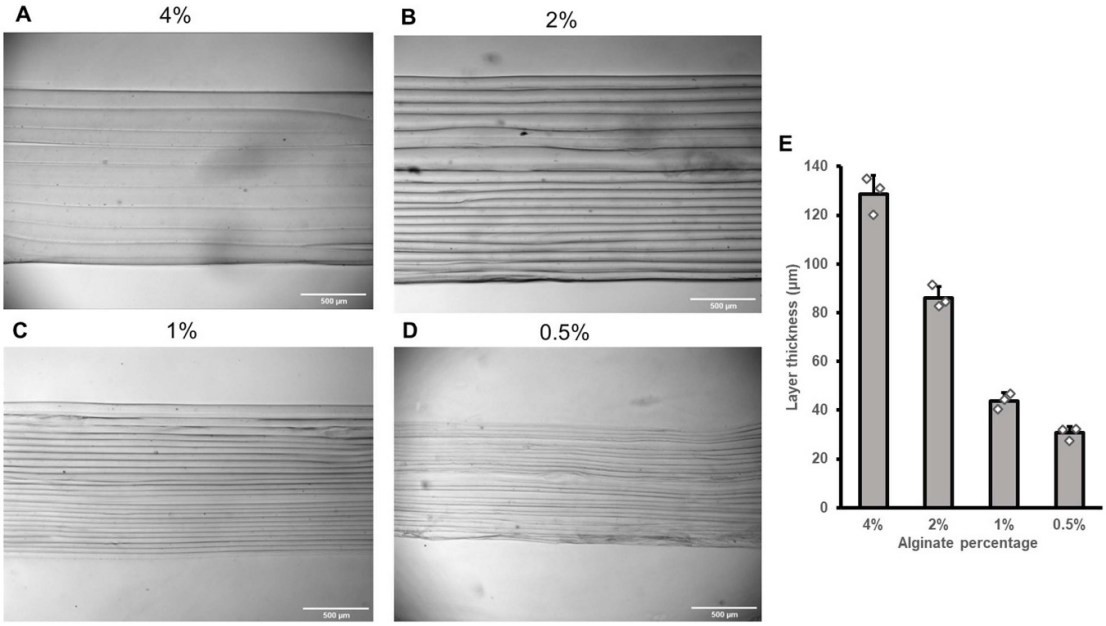

Figure 3. Alginate concentration influences the microscale layer thicknesses in tubes formed using RIFLE. Brightfield microscopy images of tubes walls with layer thicknesses and alginate concentration variation for tubes formed at 9000 rpm. Alginate percentages (w/v) (A) 4%, (B) 2%, (C) 1% and 0.5%. Scale bars are 500 μm. (E) Plot of layer thicknesses for alginate concentration variation. Mean with error bars $\pm$SD, $n = 3$.

phase in a stable layer prior to addition of a gelation agent or temperature change.

3.4. Mechanical testing

A comparison between the mechanical properties of plain unlayered tubes created by centrifugal casting (figure S4(A)) and layered RIFLE created tubes (figure S4(B)) was made. A constant strain of 5.5% was applied to tube sections mounted onto myograph wires and the relaxation force profile recorded for 10 min. Comparison of the peak forces following extension application in the two tube types was found to be not significantly different (figure S4(C)). Only minor divergences were observed between the relaxation profiles (figure S4(D)). These data show that the layers provide no clear mechanical benefit. However, the parameters tested were narrow, particularly in the context of the varied architecture seen across layered tissue in human anatomy, where cells and the ECM contribute to the mechanical properties [51]. The mechanical demands of tissue also varies considerably according to type with highly variable dynamic compressive, tensile and pulsatile loading regimes [52]. It should also be noted that stratified tissue never has a solely mechanical function, also having dynamic, barrier or sensory capabilities [53]. Furthermore, the mechanical demands of some tissue types, such as retinal tissue, is not fully understood [54]. The contribution of layers to the mechanical properties of tissue will therefore require specific experimental design for specific tissue types.

3.5. Encapsulated cell viability

Following development of the stratification process we sought to determine if cells could be included in microscale layers. HEK cells are widely used throughout biological research and were used as a proof-of-concept cell line for encapsulation, viability and positioning studies. HEK cells encapsulated into 1% (w/v) alginate layers were shown to have a viability of 97.5 $\pm$ 0.4% 24 h after RIFLE formation. The proportion of viable cells decreased in subsequent days to 60.4 $\pm$ 1.2% at day 10 (figure 4(E)). The reduction in viabilities may be attributed to the formation of necrotic cores as cells proliferated and transitioned into larger spheroid bodies [55] and has been previously observed in encapsulation protocols using alginate, ultimately limiting the tissue engineering applications the material can be used for [29, 56]. The impact of centrifugation on cells was assessed by rotating HEK cells suspended in media in a mould at 9000 rpm for 5 min. After seeding on cell culture plates these cells proliferated for 10 d and showed no clear detrimental effects from centrifugation (figure S3).

The data indicate that the overall forming protocol of trypsinisation, pelletisation, suspension in alginate and the RIFLE process results in a high cell viability with similar percentages to those attained using extrusion bioprinting, the most common biofabrication technology [57, 58]. Other cylindrical biofabrication methods have presented viabilities in the first 24 h after formation of 80% for rod dipping [29], 95% for closed cylinder centrifugal casting [31] and 20% to 60% for electrospinning

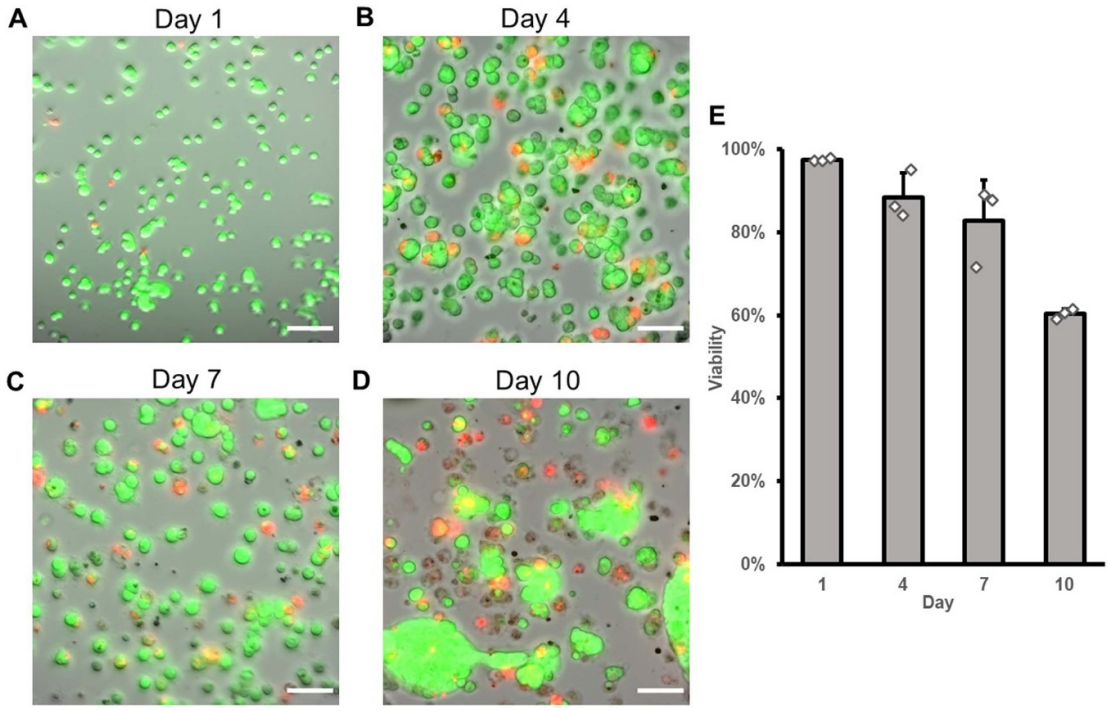

Figure 4. HEK cell viabilities following encapsulation into layers using RIFLE. Combined brightfield and fluorescent microscopy images showing HEK cell in tubes formed at 9000 rpm, 1% alginate (W/V). Live (green) and dead (red) cells at (A) day 1, (B) day 4, (C) day 7 and (D) day 10. Scale bars are 100 μm. (E) Plot of cell viability data following layer encapsulation. Mean with error bars $\pm$SD, $n = 3$.

[59]. Throughout the RIFLE process cells are subjected to centrifugal forces arising from tube rotation and also shear forces from fluid flow. Centrifugation of media suspended cells within the RIFLE mould showed no evidence of causing cell death. Simple centrifugal force calculations also reveal that a single cell is subjected to forces an order of magnitude lower than standard centrifugation used during pelletisation (1.55×10^{-11} N vs 1.22×10^{-10} N). Shear forces are also believed to have a detrimental impact on cell viability with Mironov *et al* proposing that shear forces arising from cell transfer rather than centrifugal forces were responsible for cell death in their closed cylinder system [31]. The viability data demonstrates that shear forces are low enough for cell survival and indicates that cell encapsulation at higher rotational speeds than those presented here may be feasible in the future.

3.6. Encapsulated cell layer positioning

Labelled high-density HEK cell populations—10^8 cells ml^{-1}—were assembled in varying patterns of 28 rainbow colours (figure 5(A)), alternating red and green single (figure 5(B)), double (figure 5(D)), and triple (figure 5(E)) banded layers. Confocal microscopy in the sagittal plane revealed patterned layers of, red, green and rainbow colours cell populations, as assembled. Labelled red and green cells were also assembled in tubes with 10 and 5 acellular layers between them. Combined fluorescent and brightfield microscopy of the bioassembled tubes showed encapsulated cells populations distanced by 10 (figure 5(F)) and 5 (figure 5(G)) distinct layers, also as assembled. The results confirm that each cell layer is formed as an individual process and is discrete from the surrounding adjacent layers, allowing the formation of heterogenous composite layered structures. Within their individual layers cells were observed to be homogenously distributed with a small spacing gap between them (figure 5(C)). This gap may be the result of the cross-linker addition or a function of the cell laden hydrogel flow conditions. High-density cell layers were found to be thicker than acellular and low-density layers. Previous studies have highlighted a positive correlation between cell density and hydrogel viscosity [60], with the effect here that the RIFLE process forms thicker layers. The low volume of hydrogel needed for individual layer assembly enables high density cell encapsulation to be attained. The presented density of 10^8 cells ml^{-1} aligns with observations in native cardiac tissue [61] and is at least an order of magnitude higher than previous tubular biofabrication technologies that require large volumes for emersion, spraying or extrusion [27–29, 62]. The multilayer biofabrication capability shown in the data also compares favourably with the centrifugal casting method where only a single cell layer was formed [26].

Stratified tissue varies considerably throughout mammalian anatomy, with multiple combinational

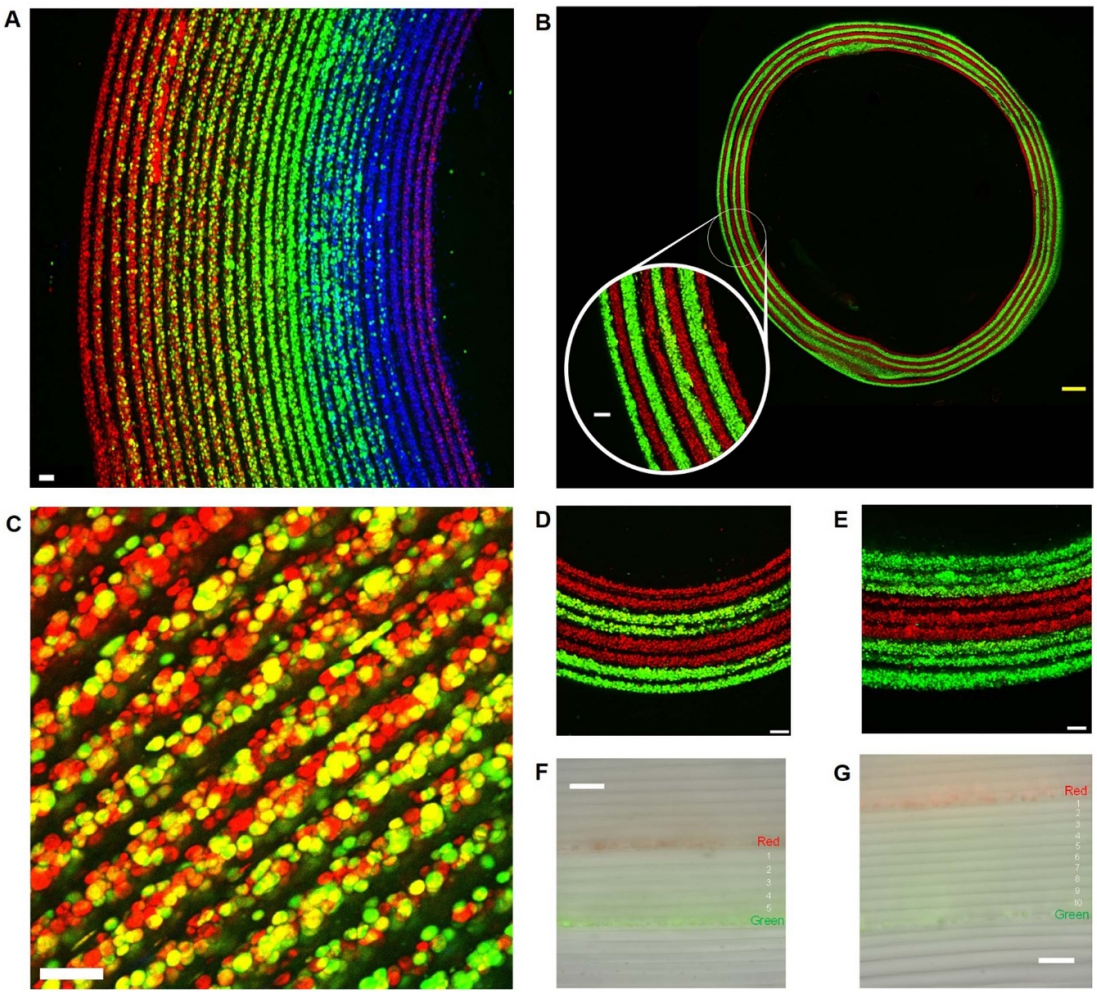

Figure 5. Cell layer positioning using RIFLE. (A), (B), (C), (D) and (E) Sagittal plane confocal images of patterned layers made using prelabelled red, green and blue high density HEK cells (10^8 cells ml^{-1}) in 1% alginate (w/v) tubes. (F) and (G) Combined brightfield and fluorescent microscopy images in the transverse plane showing the position of red and green cell layers relative to one another with 5 or 10 acellular layers between as indicated. White scale bars are 100 μm, yellow scale bar is 500 μm.

cell types, matrices and microlayer anatomy thicknesses. The data shows the bioassembly of high-density cells into microscale heterogenous structures, highlighting the potential to form a range of representative stratified 3D tissue. The precise spatial distancing of independent cell populations from one another may also have applications beyond tissue engineering, such as in the investigation of cell-to-cell signalling.

3.7. Vascular tunica media tissue engineering with RIFLE

We sought to obtain data to determine if RIFLE was able to form the microscale layers observed in vascular tubular structures. To achieve this, we aimed to biofabricate the microscale layers that make up the central tunica media, a band that is subdivided into further concentric, cell-width, strata of hSMCs, known as the medial lamellar unit [51, 63]. Collagen hydrogel, the dominant native ECM material, and also hSMCs, the native cell type for the tunica media layer were used. The same equipment for alginate bioassembly was used but with the process carried out in a 37 °C environment. A 3 min gelation time was applied for each collagen layer rather than the ionic crosslinker addition for alginate. Liquid neutralised collagen was observed spreading over the inner rotating surface of the tube with excess exiting from the drain holes in the same fashion as alginate. The macroarchitecture of completed collagen tubes was a tubular shape with an opaque white appearance (figure 6(A)). Acellular tubes formed showed evidence of microscale layer formation when viewed using brightfield microscopy. However, visualisation of layers was more difficult in comparison to alginate tubes due to the opacity of the gelled collagen, with layers of ≈15 μm visible on the outer edge of the wall (figure 6(B)). The requirement to allow each layer 3 min to gel extends the bioassembly time, with 25 collagen layers taking approximately 1.5 h.

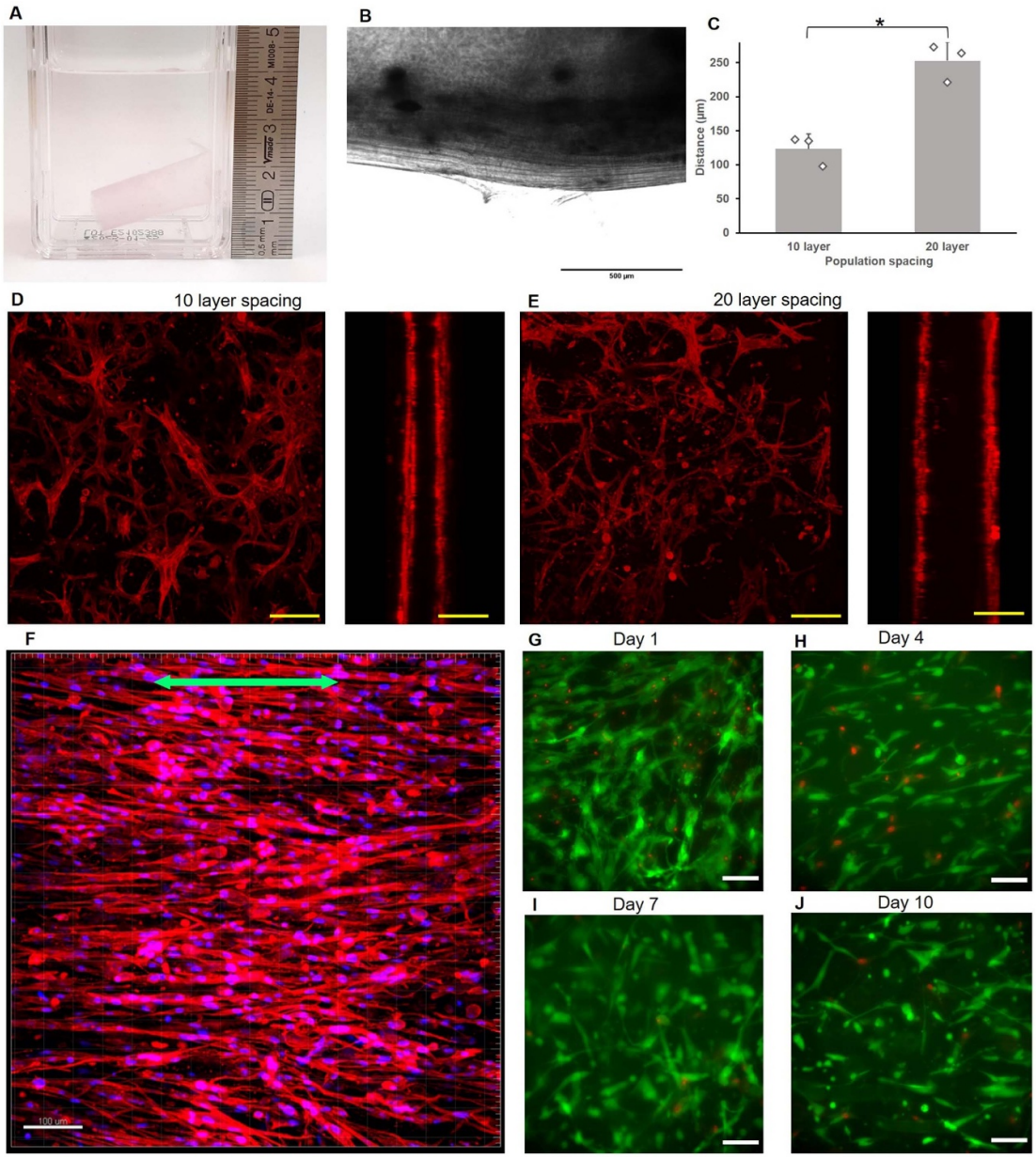

Figure 6. Bioassembly of vascular tunica media tissue using RIFLE. (A) Macroscale collagen tube architecture with an opaque appearance. (B) Light microscopy of microscale acellular collagen layer formation. Black scale bar is 500 μm. (C) Plot of measured distances between hSMC layers for the 10 and 20 layer groups. Mean with error bars $\pm$SD, $n = 3$, two-sided student t test. $^{*}P < 0.005$. (D) and (E) Confocal stacks in the sagittal and transverse planes showing F-actin stained (phalloidin, red) hSMCs layers positioned with 20 and 10 acellular layer spacing. Yellow scale bars are 200 μm. (F) hSMC orientation 4 d after stratification. F-actin (phalloidin, red) nuclei (Hoechst, blue). Green arrow indicates circumferential direction. White scale bar is 100 μm (G)–(J) Single layer hSMC viability in collagen. Live (green) and dead (red) cells at 1, 4, 7 and 10 d post assembly. White scale bars are 100 μm.

To bioassemble the vascular tunica media, hSMCs were suspended in neutralised collagen prior to addition to the inner surface of the rotating mould. hSMCs added as a single layer amongst acellular layers demonstrated viability for up to 10 d post assembly (figures 6(G)–(J)). Timelapse videos of hSMCs in the first 24 h after bioassembly showed the cells transitioning from a spherical to a spread morphology in the plane of the layer (supplementary movie 2). Macroscale tubes containing hSMCs encapsulated in all layers were allowed to compact onto an inner mandrel after bioassembly to prevent over shrinkage of the tube as viable cells haul up surrounding collagen fibrils [64]. The compaction onto the mandrel was observed to happen within the first 24 h and the tubes were removed after 4 d of culture. Upon release from the mandrel F-actin visualisation revealed a network of hSMCs aligned in the circumferential direction (figure 6(F)). Such cellular orientation closely mimics the microscale organisation observed in native vascular tissue [18]. The clamping of the layered tube onto the mandrel arising from the compaction process will have created static tensile forces in the circumferential direction. The orientation of SMCs encapsulated

in collagen in the direction of static tension has been previously shown [65] and it is likely that the layered hSMCs are exhibiting the same behaviour.

To determine the thickness of assembled collagen layers, independent populations of hSMCs were assembled with 10 or 20 acellular layers spaced between them. F-actin visualisation via phalloidin staining and confocal microscopy revealed spread hSMCs in two distanced, independent, narrow cell-width microscale layers (figures 6(D) and (E) and supplementary movies 3 and 4). The distance between cell layers in the 10 and 20 layer assemblies increased proportionately (figure 6(C)), with an average layer thickness of 12.5 $\pm$ 1.7 μm. This distance closely matches published measurements of the thickness of the native medial lamellar unit, recorded at 13.9 $\pm$ 1.2 μm (rat) [18] and 13.2 μm (human) [63]. The assembly of viable hSMCs into concentric, anatomically accurate layers represents an important progression for vascular biofabrication technologies. Bioprinting studies frequently only refer to the macrolayers of the tunica intima, media or adventitia, oversimplifying the complex microtissue layered architecture within these structures, such as the medial lamellar unit [18, 51, 63, 66]. The results show that RIFLE is able encapsulate vascular cells in anatomically accurate concentric medial lamellar units in the native ECM material of collagen.

There remain several limitations of the assembled tunica media tissue in comparison to native tissue. The constructs do not feature the elastin lamellar that lie between the medial lamellar units [18]. These sheets are believed to significantly contribute to the mechanical strength of vessel walls [67]. The degradation profile of a biofabricated structure is essential to its long-term patency and would need to be assessed for any tissue created using RIFLE. The long-term stability in an *in-vivo* or representative *in-vivo* environment will therefore need assessing for a particular layered cell and hydrogel combination. No evidence of collagen layer delamination was observed with tube walls remaining together throughout the culture stages. However, the delamination of the collagen layers when exposed to forces and strains, as would be induced *in-vivo* by pulsatile blood flow, is a possible failure mode and will require further study. The inclusion of the surrounding adventitia, intima and endothelia along with their respective cell types and ECMs would also be needed to faithfully recreate the *in-vivo* environment. In addition, we have only tested a simple tubular shape whereas native macroscale tissue can be more complex, such as vascular bifurcations and ventricular bodies. The industrial process of rotational moulding utilises rimming flow in hollow moulds with complex geometries. Further investigation will be required to determine if more complex multi-layered macroscale geometry can be created using the RIFLE principle of rimming flow.

The data provides evidence that the RIFLE system can be directed towards vascular tissue engineering via the thermal gelation of microscale collagen layers into the medial lamellar unit. Microstratification of cells encapsulated in collagen is also significant for other tissue engineering applications, being the principal component of most extracellular matrices and accounts for 30% of human protein mass [68]. Furthermore, collagen has typically proved difficult to manipulate using existing bioassembly technologies [69]. This is due to a combination of low viscosity and extended thermal gelation time [21, 70], ultimately requiring a high level of self-support and temperature control when transitioning from a liquid to a gel [71, 72] a challenge prevalent throughout biofabrication, with technologies often requiring specific bioink hydrogel formulations. Collagen itself is often combined with other hydrogels such as alginate [73] to enable bioprinting. The RIFLE system circumvents this problem for stratified tissue with the stable suspension of the liquid phase hydrogel in the desired microscale spatial constraint prior to application of the gelation reagent or process.

3.8. Economical stratified tissue bioassembly

The described system uses simple equipment needing only the single axis rotation of a DC motor and therefore requires no complex control software or associated programming skills. The apparatus used is all readily available to research laboratories at a relatively low cost. The combined total for the equipment presented is less than $950, the majority of which is for the DC motor and controller, with cheaper versions available. The high cost of bioprinting equipment alongside required specialised expertise [74] is often a barrier to researchers seeking to assemble tissue in the laboratory [75] with current commercial options costing between $10 000 and $1000 000 [76]. It is hoped that more affordable, user-friendly technologies will enable greater access for laboratories wishing to develop engineered tissue for research and ultimately clinical purposes. The speed of layered tissue fabrication using RIFLE presents a further advantage to researchers too, especially in comparison to technologies such as cell-sheet engineering which requires extensive 2D culture [62] and maturation times [6].

4. Conclusion

In this paper we have presented RIFLE, a new technology for biofabricating cell-laden hydrogels into macroscale tubes comprised of microscale layers. Strata thicknesses were shown to be tuneable through gel viscosity and the rotational speed variation. Three hydrogels, each with a different gelation mechanism were shown to be compatible with the technology and formed microscale layers. Each

layer is formed in an individual process and is discrete from its adjacent layers allowing the potential formation of highly varied composite layered structures. Stratified tissue varies considerably throughout mammalian anatomy, with multiple combinational cell types, matrices and microlayer anatomy thicknesses. Biofabrication methods that are able to account for this variation through controlled layer deposition can have a valuable role in the future development of highly representative 3D tissue.

The described system therefore further supplements the number of emerging biofabrication technologies available to researchers seeking to mimic microscale tissue features. In this regard RIFLE can be considered to be an enabling technology for the two-step biomanufacturing roadmap outlined by Wolf *et al* [77]. Firstly, the creation of the tissue functional unit microarchitecture, the medial lamellar unit in the presented example, followed by the bioassembly of these units into a bulk tissue, here a macroscale tube. It is hoped that the future use of RIFLE will facilitate others to repeat this approach for a range of different stratified tissue types.

Data availability statement

The data that support the findings of this study are openly available at the following URL/DOI: https://doi.org/10.7488/ds/7475.

Acknowledgments

We would like to thank Anisha Kubasik-Thayil at the University of Edinburgh IMPACT Imaging Facility.

Funding

We would like to acknowledge the following funding. I H and J D European Research Council (ERC) under the European Union's Horizon 2020 research and innovation scheme (Grant Agreement No. 801041, Cyber Genetic Tissue Engineering). I H and W S UK Engineering & Physical Sciences Research Council (EPSRC) Doctoral Prize Fellowship (Grant No. EP/N509760/1). I H and J D UK Biotechnology & Biological Science Research Council (BBSRC) (Grant Agreement No. BB/M018040/1).

Conflict of interest

The University of Edinburgh has filed for patent protection on the technology described herein, and I H, W S and J D are named as inventors on the patent.

Author contributions

I H, W S and J D designed the research. I H performed the experiments, analysed the data and wrote the manuscript with input from W S and J D.

ORCID iDs

Ian Holland https://orcid.org/0000-0002-8728-7117
Wenmiao Shu https://orcid.org/0000-0002-1220-361X

References

[1] Tsukamoto Y, Akagi T and Akashi M 2020 Vascularized cardiac tissue construction with orientation by layer-by-layer method and 3D printer *Sci. Rep.* **10** 1–3
[2] Savoji H, Godau B, Hassani M S and Akbari M 2018 Skin tissue substitutes and biomaterial risk assessment and testing *Front. Bioeng. Biotechnol.* **6** 1–18
[3] Clevers H, Conder R K, Vsw L, Lutolf M P, Vallier L, Chan S, Grikscheit T C, Jensen K B and de Coppi P 2019 Tissue-engineering the intestine: the trials before the trials *Cell Stem Cell* **24** 855–9
[4] Marcos L F, Wilson S L and Roach P 2021 Tissue engineering of the retina: from organoids to microfluidic chips *J. Tissue Eng.* **12** 20417314211059876
[5] Ng W L, Ayi T C, Liu Y C, Sing S L, Yeong W Y and Tan B H 2021 Fabrication and characterization of 3D bioprinted triple-layered human alveolar lung models *Int. J Bioprinting* **7** 1–15
[6] Fazal F, Raghav S, Callanan A, Koutsos V and Radacsi N 2021 Recent advancements in the bioprinting of vascular grafts *Biofabrication* **13** 032003
[7] Sun W *et al* 2020 The bioprinting roadmap *Biofabrication* **12** 022002
[8] Groll J *et al* 2016 Biofabrication: reappraising the definition of an evolving field *Biofabrication* **8** 013001
[9] Moroni L, Boland T, Burdick J A, de Maria C, Derby B, Forgacs G and Vozzi G 2017 Biofabrication: a guide to technology and terminology *Trends Biotechnol.* **36** 1–19
[10] Spicer C D 2020 Hydrogel scaffolds for tissue engineering: the importance of polymer choice *Polym. Chem.* **11** 184–219
[11] Li X, Liu B, Pei B, Chen J, Zhou D, Peng J, Zhang X, Jia W and Xu T 2020 Inkjet bioprinting of biomaterials *Chem. Rev.* **120** 10793–833
[12] Morgan F L C, Moroni L and Baker M B 2020 Dynamic bioinks to advance bioprinting *Adv. Healthcare Mater.* **9** 1901798
[13] Ng W L, Lee J M, Zhou M, Chen Y W, Lee K X A, Yeong W Y and Shen Y-F 2020 Vat polymerization-based bioprinting—process, materials, applications and regulatory challenges *Biofabrication* **12** 022001
[14] Li W, Mille L S, Robledo J A, Uribe T, Huerta V and Zhang Y S 2020 Recent advances in formulating and processing biomaterial inks for vat polymerization-based 3D printing *Adv. Healthcare Mater.* **9** 2000156
[15] Santoni S, Gugliandolo S G, Sponchioni M, Moscatelli D and Colosimo B M 2022 3D bioprinting: current status and trends—a guide to the literature and industrial practice *Bio-Des. Manuf.* **5** 14–42
[16] Maeng W, Tseng W, Li S, Koo J and Hsueh Y 2022 Electroceuticals for peripheral nerve regeneration *Biofabrication* **14** 042002
[17] Jafari A, Ajji Z, Mousavi A, Naghieh S, Bencherif S A and Savoji H 2022 Latest advances in 3D bioprinting of cardiac tissues *Adv. Mater. Technol.* **7** 1–24
[18] O'Connell M K, Murthy S, Phan S, Xu C, Buchanan J A, Spilker R, Dalman R, Zarins C, Denk W and Taylor C 2008 The three-dimensional micro- and nanostructure of the aortic medial lamellar unit measured using 3D confocal and electron microscopy imaging *Matrix Biol.* **27** 171–81
[19] Malda J, Visser J, Melchels F P, Jüngst T, Hennink W E, Dhert W J A, Groll J and Hutmacher D W 2013 25th anniversary article: engineering hydrogels for biofabrication *Adv. Mater.* **25** 5011–28

[20] Rodríguez-Rego J M, Mendoza-Cerezo L, Macías-García A, Carrasco-Amador J P and Marcos-Romero A C 2023 Methodology for characterizing the printability of hydrogels *Int. J. Bioprint.* **9** 667
[21] Fu Z, Naghieh S, Xu C, Wang C, Sun W and Chen X 2021 Printability in extrusion bioprinting *Biofabrication* **13** 033001
[22] Harley W S, Li C C, Toombs J, O'Connell C D, Taylor H K, Heath D E and Collins D J 2021 Advances in biofabrication techniques towards functional bioprinted heterogeneous engineered tissues: a comprehensive review *Bioprinting* **23** e00147
[23] Holland I, Logan J, Shi J, McCormick C, Liu D and Shu W 2018 3D biofabrication for tubular tissue engineering *Bio-Des. Manuf.* **1** 89–100
[24] Sampaziotis F *et al* 2017 Reconstruction of the mouse extrahepatic biliary tree using primary human extrahepatic cholangiocyte organoids *Nat. Med.* **23** 954–63
[25] Boys A J, Barron S L, Tilev D and Owens R M 2020 Building scaffolds for tubular tissue engineering *Front. Bioeng. Biotechnol.* **8** 1–20
[26] Mironov V, Kasyanov V, Markwald R R and Prestwich G D 2008 Bioreactor-free tissue engineering: directed tissue assembly by centrifugal casting *Expert Opin. Biol. Ther.* **8** 143–52
[27] Wilkens C A, Rivet C J, Akentjew T L, Alverio J, Khoury M and Acevedo J P 2017 Layer-by-layer approach for a uniformed fabrication of a cell patterned vessel-like construct *Biofabrication* **9** 015001
[28] Akentjew T L *et al* 2019 Rapid fabrication of reinforced and cell-laden vascular grafts structurally inspired by human coronary arteries *Nat. Commun.* **10** 3098
[29] Ghanizadeh Tabriz A, Mills C G, Mullins J J, Davies J A and Shu W 2017 Rapid fabrication of cell-laden alginate hydrogel 3D structures by micro dip-coating *Front. Bioeng. Biotechnol.* **5** 13
[30] Kasyanov V A *et al* 2009 Rapid biofabrication of tubular tissue constructs by centrifugal casting in a decellularized natural scaffold with laser-machined micropores *J. Mater. Sci. Mater. Med.* **20** 329–37
[31] Mironov V, Kasyanov V, Xiao Z S, Eisenberg C, Eisenberg L, Gonda S, Trusk T, Markwald R R and Prestwich G D 2005 Fabrication of tubular tissue constructs by centrifugal casting of cells suspended in an *in situ* crosslinkable hyaluronan-gelatin hydrogel *Biomaterials* **26** 7628–35
[32] Skylar-Scott M A, Uzel S G M, Nam L L, Ahrens J H, Truby R L, Damaraju S and Lewis J A 2019 Biomanufacturing of organ-specific tissues with high cellular density and embedded vascular channels *Sci. Adv.* **5** eaaw2459
[33] Baviskar S N 2011 A quick & automated method for measuring cell area using ImageJ *Am. Biol. Teach.* **73** 554–6
[34] Park J A *et al* 2017 Freeform micropatterning of living cells into cell culture medium using direct inkjet printing *Sci. Rep.* **7** 1–11
[35] Ruschak K J and Scriven L E 1976 Rimming flow of liquid in a rotating cylinder *J. Fluid Mech.* **76** 113–26
[36] Ogila K O, Shao M, Yang W and Tan J 2017 Rotational molding: a review of the models and materials *Express Polym. Lett.* **11** 778–98
[37] Preziosi L and Joseph D D 1988 The run-off condition for coating and rimming flows *J. Fluid Mech.* **187** 99–113
[38] Sadeghi H, Diosady L and Blais B 2022 A computational fluid dynamics study on rimming flow in a rotating cylinder *Phys. Fluids* **34** 063304
[39] Mitchell A J, Duffy B R and Wilson S K 2022 Unsteady coating flow on a rotating cylinder in the presence of an irrotational airflow with circulation *Phys. Fluids* **34** 043105
[40] Chen P-J, Tsai Y-T, Liu T-J and Wu T-Y 2007 Low volume fraction rimming flow in a rotating horizontal cylinder *Phys. Fluids* **19** 128107
[41] Chicharro R, Vazquez A and Manasseh R 2011 Characterization of patterns in rimming flow *Exp. Therm. Fluid Sci.* **35** 1184–92
[42] Pougatch K and Frigaard I 2011 Thin film flow on the inside surface of a horizontally rotating cylinder: steady state solutions and their stability *Phys. Fluids* **23** 022102
[43] Harkin-Jones E and Crawford R 1996 Rotational molding of liquid plastic systems: an assessment of material moldability *Adv. Polym. Technol.* **15** 71–100
[44] Axpe E and Oyen M 2016 Applications of alginate-based bioinks in 3D bioprinting *Int. J. Mol. Sci.* **17** 1976
[45] Freeman F E and Kelly D J 2017 Tuning alginate bioink stiffness and composition for controlled growth factor delivery and to spatially direct MSC fate within bioprinted tissues *Sci. Rep.* **7** 1–12
[46] Fernández E, López D, Mijangos C, Duskova-Smrckova M, Ilavsky M and Dusek K 2008 Rheological and thermal properties of agarose aqueous solutions and hydrogels *J. Polym. Sci.* B **46** 322–8
[47] Thoroddsen S T and Mahadevan L 1997 Experimental study of coating flows in a partially-filled horizontally rotating cylinder *Exp. Fluids* **23** 1–13
[48] Kong H J, Kaigler D, Kim K and Mooney D J 2004 Controlling rigidity and degradation of alginate hydrogels via molecular weight distribution *Biomacromolecules* **5** 1720–7
[49] Vázquez-Aristizabal P, Perumal G, García-Astrain C, Liz-Marzán L M and Izeta A 2022 Trends in tissue bioprinting, cell-laden bioink formulation, and cell tracking *ACS Omega* **7** 16236–43
[50] Sarmin A M and Connelly J T 2022 Fabrication of human skin equivalents using decellularized extracellular matrix *Curr. Protocols* **2** 1–10
[51] Akhtar R, Sherratt M J, Cruickshank J K and Derby B 2011 Characterizing the elastic properties of tissues *Mater. Today* **14** 96–105
[52] Liebschner M, Bucklen B and Wettergreen M 2005 Mechanical aspects of tissue engineering *Semin. Plast. Surg.* **19** 217–28
[53] Biggs L C, Kim C S, Miroshnikova Y A and Wickstro S A 2020 Mechanical forces in the skin: roles in tissue architecture, stability, and function *J. Invest. Dermatol.* **140** 284–90
[54] Ferrara M, Lugano G, Sandinha M T, Kearns V R, Geraghty B and Steel D H W 2021 Biomechanical properties of retina and choroid: a comprehensive review of techniques and translational relevance *Eye* **35** 1818–32
[55] Štampar M, Breznik B, Filipič M and Žegura B 2020 Characterization of *in vitro* 3D cell model developed from human hepatocellular carcinoma (HepG2) cell line *Cells* **9** 2557
[56] Karpov A A, Puzanov M V, Ivkin D Y, Krasnova M V, Anikin N A, Docshin P M, Moiseeva O M and Galagudza M M 2019 Non-inferiority of microencapsulated mesenchymal stem cells to free cells in cardiac repair after myocardial infarction: a rationale for using paracrine factor(s) instead of cells *Int. J. Exp. Pathol.* **100** 102–13
[57] Bociaga D, Bartniak M, Grabarczyk J and Przybyszewska K 2019 Sodium alginate/gelatine hydrogels for direct bioprinting-the effect of composition selection and applied solvents on the bioink properties *Materials* **12** 1–19
[58] Ozbolat I T and Hospodiuk M 2016 Current advances and future perspectives in extrusion-based bioprinting *Biomaterials* **76** 321–43
[59] Xue J, Wu T, Dai Y and Xia Y 2019 Electrospinning and electrospun nanofibers: methods, materials, and applications *Chem. Rev.* **119** 5298–415
[60] Cao N, Chen X B and Schreyer D J 2012 Influence of calcium ions on cell survival and proliferation in the context of an alginate hydrogel *ISRN Chem. Eng.* **2012** 1–9
[61] Radisic M, Euloth M, Yang L, Langer R, Freed L E and Vunjak-Novakovic G 2003 High-density seeding of myocyte

cells for cardiac tissue engineering *Biotechnol. Bioeng.* **82** 403–14
[62] Freeman S, Ramos R, Alexis Chando P, Zhou L, Reeser K, Jin S, Soman P and Ye K 2019 A bioink blend for rotary 3D bioprinting tissue engineered small-diameter vascular constructs *Acta Biomater.* **95** 152–64
[63] Tracy R E, Kissling G E and Curtis M B 1987 Smooth muscle cell—reticulin lamellar units of 13.2 microns thickness composing the aortic intima *Virchows Arch.* A **411** 415–24
[64] van den Akker J, Tuna B G, Pistea A, Sleutel A J J, Entp B and van Bavel E 2012 Vascular smooth muscle cells remodel collagen matrices by long-distance action and anisotropic interaction *Med. Biol. Eng. Comput.* **50** 701–15
[65] Kanda K and Matsuda T 1994 Mechanical stress-induced orientation and ultrastructural change of smooth muscle cells cultured in three-dimensional collagen lattices *Cell Transplant.* **3** 481–92
[66] Cocciolone A J, Hawes J Z, Staiculescu M C, Johnson E O, Murshed M and Wagenseil J E 2018 Elastin, arterial mechanics, and cardiovascular disease *Am. J. Physiol. Heart Circ. Physiol.* **315** H189–205
[67] Mozafari H, Zhou C and Gu L 2019 Mechanical contribution of vascular smooth muscle cells in the tunica media of artery *Nanotechnol. Rev.* **8** 50–60
[68] Abraham L C, Zuena E, Perez-Ramirez B and Kaplan D L 2008 Guide to collagen characterization for biomaterial studies *J. Biomed. Mater. Res.* B **87** 264–85
[69] Lee A, Hudson A R, Shiwarski D J, Tashman J W, Hinton T J, Yerneni S, Bliley J M, Campbell P G and Feinberg A W 2019 3D bioprinting of collagen to rebuild components of the human heart *Science* **365** 482–7
[70] Lee G, Kim S J, Chun H and Park J K 2021 Multilayered and heterogeneous hydrogel construct printing system with crosslinking aerosol *Biofabrication* **13** 045027
[71] Suo H, Zhang J, Xu M and Wang L 2021 Low-temperature 3D printing of collagen and chitosan composite for tissue engineering *Mater. Sci. Eng.* C **123** 111963
[72] Stepanovska J, Supova M, Hanzalek K, Broz A and Matejka R 2021 Collagen bioinks for bioprinting: a systematic review of hydrogel properties, bioprinting parameters, protocols, and bioprinted structure characteristics *Biomedicines* **9** 1137
[73] Dogan L, Scheuring R, Wagner N, Ueda Y, Schmidt S, Wörsdörfer P, Groll J and Ergün S 2021 Human iPSC-derived mesodermal progenitor cells preserve their vasculogenesis potential after extrusion and form hierarchically organized blood vessels *Biofabrication* **13** 045028
[74] Hinton T J, Jallerat Q, Palchesko R N, Park J H, Grodzicki M S, Shue H-J, Ramadan M H, Hudson A R and Feinberg A W 2015 Three-dimensional printing of complex biological structures by freeform reversible embedding of suspended hydrogels *Sci. Adv.* **1** e1500758
[75] Wagner M, Karner A, Gattringer P, Buchegger B and Hochreiner A 2021 A super low-cost bioprinter based on DVD-drive components and a raspberry pi as controller *Bioprinting* **23** e00142
[76] Chimene D, Deo K A, Thomas J, Dahle L, Mandrona C and Gaharwar A K 2022 Designing cost-effective open-source multihead 3D bioprinters *GEN Biotechnol.* **1** 386–400
[77] Wolf K J, Weiss J D, Uzel S G M, Skylar-Scott M A and Lewis J A 2022 Biomanufacturing human tissues via organ building blocks *Cell Stem Cell.* **29** 667–77